Upper-Ocean Inertial Currents Forced by a Strong Storm. Part III: Interaction of Inertial Currents and Mesoscale Eddies*

ERIC A. D'ASARO

Applied Physics Laboratory, College of Ocean and Fishery Sciences, University of Washington, Seattle, Washington

(Manuscript received 25 April 1994, in final form 22 May 1995)

ABSTRACT

The interaction of strong near-inertial frequency currents generated by a storm with preexisting subinertial frequency currents is investigated. For 10 days after the storm, the near-inertial currents remain in the mixed layer and the subinertial currents are steady, so their interaction is particularly simple. Linearized models predict that the frequency of the near-inertial currents should be shifted by $\frac{1}{2}\zeta$, where ζ is the subinertial vorticity. This theory, combined with values of ζ estimated either from velocity measurements or from the vorticity equation, produces frequency shifts in the inertial currents at least five times larger than the confidence limits on the observations. Possible explanations include the concentration of ζ in narrow frontal zones and nonlinear wave–wave interactions.

1. Introduction

Near-inertial frequency currents are the most energetic part of the oceanic internal wave spectrum and are commonly observed throughout the ocean depth. Although considerable insight into their properties can be obtained by considering them to be linear waves propagating in a homogeneous ocean, the inhomogeneity of the ocean probably cannot be ignored. For example, Kunze (1985) uses ray theory to demonstrate the importance of the parameter

$$f_{\text{eff}} = f + \frac{1}{2}\zeta. \tag{1}$$

In the presence of background geostrophic velocities, the frequency of near-inertial waves is shifted by an amount $\frac{1}{2}\zeta$, so that pure inertial motions have the frequency f_{eff}, rather than the Coriolis frequency f. Spatial variations in f_{eff} refract near-inertial waves, sometimes leading to trapping, amplification, and enhanced mixing. Some of these effects have been found in the ocean (Kunze and Sanford 1984; Mied et al. 1987; Kunze et al. 1995).

Part I of this paper (D'Asaro et al. 1995a) describes the structure and evolution of near-inertial currents generated in the mixed layer of the northeast Pacific by a strong storm. The storm has a large horizontal scale and moves rapidly over the experimental area, so the near-inertial currents that it generates are nearly uniform over the 300-km-square measurement array. The wind is weak for 20 days following the storm. The vertical propagation of these inertial motions from the mixed layer into the thermocline as linear internal waves is quite slow, owing to their large horizontal scale. This scale steadily decreases because of the β effect, increasing the rate of wave propagation. By 10 days after the storm the mixed layer inertial motions have a wavelength of about 600 km, and wave propagation has reduced their energy to about half of its initial value. This paper will concentrate on the first 10 days after the storm when the inertial motions are mostly confined to the mixed layer.

The subinertial frequency currents in this same region are also described in Part I. During the period of interest, the wind is weak and the subinertial mixed layer currents are steady and geostrophic. Their rms velocity is about 0.06 m s^{-1}. An objective analysis of the velocity field finds that the rms vorticity is about $0.02f$ and has a dominant wavelength of about 100 km.

These data offer an excellent opportunity to examine the interaction between inertial and subinertial currents. Since the inertial currents are confined to the mixed layer, the two-dimensional, that is, horizontal, aspects of this interaction are emphasized. This makes the theoretical problem particularly simple. Equation (1) predicts that the frequency of the mixed layer inertial motions should vary by $\frac{1}{2}\zeta$, or about $0.01f$ rms. This is equivalent to about 50° of phase change in 10 days and should be easily detectable. The main result of this

* University of Washington School of Oceanography Contribution Number 2131.

Corresponding author address: Dr. Eric A. D'Asaro, Applied Physics Laboratory, University of Washington, 1013 N.E. 40th Street, Seattle, WA 98105.
E-mail: dasaro@apl.washington.edu

paper is that no such signal is present in the observations.

Other papers in this volume contain background and complementary information. The data and data processing are described in Part I. Crawford and Large (1995) and Large and Crawford (1995) describe the storm and the generation of the mixed layer inertial currents. The propagation of these inertial motions out of the mixed layer is discussed in Parts I and II of this paper, Levine and Zervakis (1995), Zervakis and Levine (1995), and Qui et al. (1995). A numerical simulation of this propagation, with and without idealized subinertial currents, is presented in Part II (D'Asaro 1995).

2. Theory

Consider a vertically uniform mixed layer of depth H with near-inertial frequency currents $\mathbf{u} = (u, v)$ superimposed on a mesoscale eddy field with velocities $\bar{\mathbf{U}} = (\bar{U}, \bar{V})$. The Boussinesq horizontal momentum equations with no wind forcing and linearized in $\mathbf{u}$ are

$$\frac{Du}{Dt} + \mathbf{u}\cdot\nabla_H\bar{U} - fv = -\rho_0^{-1}\frac{\partial P}{\partial x} \tag{2a}$$

$$\frac{Dv}{Dt} + \mathbf{u}\cdot\nabla_H\bar{V} + fu = -\rho_0^{-1}\frac{\partial P}{\partial y}, \tag{2b}$$

where $D/Dt = \partial/\partial t + \bar{U}\cdot\nabla$. The linearization cannot be justified by scaling; $\mathbf{u}\cdot\nabla\bar{\mathbf{U}}$ is of comparable magnitude to $\mathbf{u}\cdot\nabla\bar{\mathbf{u}}$ in our data. The simulations in Part II, however, show that the nonlinearity of the inertial motions, $\mathbf{u}\cdot\nabla\bar{\mathbf{u}}$, has little systematic effect on their propagation. In contrast, it is now shown that the interaction of the inertial and subinertial currents, $\mathbf{u}\cdot\nabla\bar{\mathbf{U}}$, leads to (1), which has profound effects.

We use complex notation for the inertial motions so that

$$U = u + iv \tag{3}$$

and then add (2a) to i times (2b) and rewrite (2) as

$$\frac{DU}{Dt} + if_{\text{eff}}U + U^*(S_1 + iS_2) = P_g, \tag{4}$$

where f_{eff} is defined in (1) with vorticity $\zeta = \bar{V}_x - \bar{U}_y$; $S_1 = \frac{1}{2}(\bar{U}_x - \bar{V}_y)$ and $S_2 = \frac{1}{2}(\bar{U}_y + \bar{V}_x)$ are the mean normal and shear strain rates and subscripts have been used to denote differentiation. Note that f varies with latitude; P_g includes the two pressure terms from (2). We define the complex amplitude of the inertially demodulated current referenced to a fixed inertial frequency f_0 and time t_0:

$$U = \tilde{U}e^{-if_0(t-t_0)}. \tag{5}$$

The components of $\tilde{U}$ form the "backrotated inertial velocity vector." Similarly, the pressure gradient is written

$$P_g = \tilde{P}e^{-if_0(t-t_0)}. \tag{6}$$

In terms of these, (4) is

$$\frac{D\tilde{U}}{Dt} + i(f_{\text{eff}} - f_0)\tilde{U} + \tilde{U}^*(S_1 + iS_2)e^{2if_0(t-t_0)} = \tilde{P}. \tag{7}$$

In our data, the subinertial currents, strains, and vorticities, as well as the backrotated inertial current vectors vary on a timescale of many inertial periods from both an Eulerian and Lagrangian, that is, along trajectories, point of view. Therefore, if we average (7) over one or more inertial periods, then the strain term will average to zero, while the inertial amplitudes remain unchanged, so

$$\frac{D\tilde{U}}{Dt} + i(f_{\text{eff}} - f_0)\tilde{U} = \tilde{P}. \tag{8}$$

Equation (8) states that with no pressure gradients, the mixed inertial currents will oscillate at a frequency f_{eff} in a Lagrangian reference frame moving with the mean flow. Wave propagation, acting through $\tilde{P}$, can modify these currents. Note that $f_{\text{eff}} - f_0 = \beta(y - y_0) + \frac{1}{2}\zeta$. The mixed layer subinertial currents modify the mixed layer inertial currents by advecting them and by shifting their frequency by $\frac{1}{2}\zeta$.

Wave propagation is weak during our analysis period. We therefore ignore $\tilde{P}$ in (8) and rewrite it as

$$\tilde{U}(t) = \tilde{U}(t_1) + \int_{t_1}^{t} i(f_{\text{eff}} - f_0)\tilde{U}dt, \tag{9}$$

where the integration is along a Lagrangian trajectory. Our analysis will consist of comparing (9) with the observed evolution of the mixed layer inertial currents.

Wave propagation, however, does occur during our analysis period, reducing the energy of the mixed layer inertial currents by about half. Linear theory (see Part I) predicts that the rate of wave propagation is proportional to

$$\tilde{k}^2 \equiv \frac{\nabla^2\tilde{U}}{|\tilde{U}|} \tag{10}$$

so that inertial currents with small horizontal scales propagate faster than those with large scales. Numerically, the inertial motions in the mixed layer of our data have $\tilde{k}^{-1}$ of about 100 km, corresponding to their approximately 10-day residence time in the mixed layer. We will use (9) to estimate the change in $\tilde{k}$ due to the geostrophic currents and then use (10) plus linear theory to estimate the additional effects of wave propagation.

3. Observations

a. Inertial currents

Estimates of the mixed layer inertial current $\tilde{U}$ demodulated to the inertial frequency at 47.5°N and back-

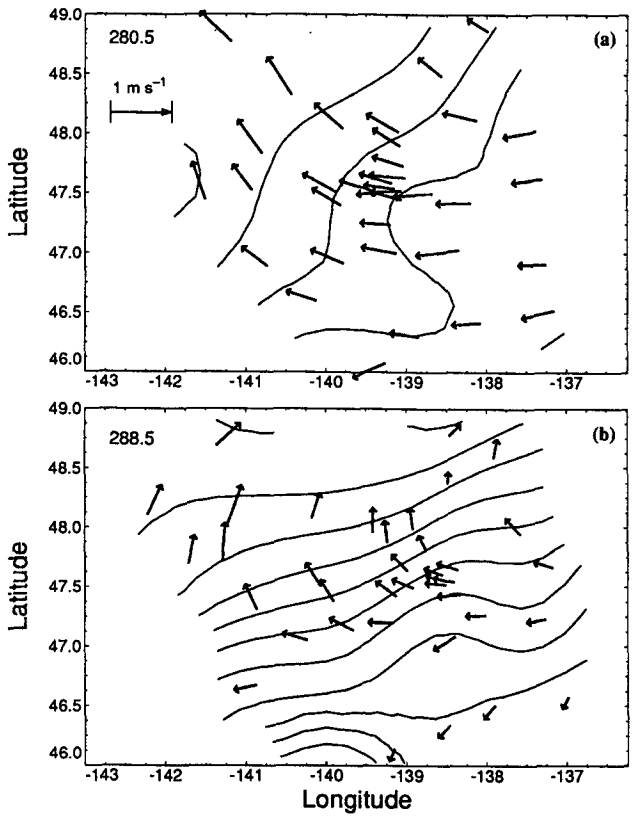

FIG. 1. Observed mixed layer backrotated inertial current vectors on (a) day 280.5 and (b) day 288.5. Vector direction is contoured with interval of 22.5°.

rotated [see (5)] to t_0 = day 278.0 of 1987 were made along the trajectories of 31 surface drifters drogued at 15 m (see Part I). Figure 1a shows backrotated inertial current vectors on day 280.5 of 1987, two days after the storm, while Fig. 1b shows these vectors on day 288.5. Their direction, or equivalently the phase of the demodulated inertial currents, is contoured. The horizontal scale of the inertial currents decreases by about a factor of 4 between days 280.5 and 288.5, owing to β, and their amplitude decreases by about 30%, owing to wave propagation, as described in Part I.

At both times, the amplitude of the inertial currents is nearly constant in space and the phase varies nearly linearly. Most of the energy in the inertial velocity field can therefore be described by fitting a single plane wave to the data

$$\tilde{U}(x, y) = \tilde{U}_{\text{fit}} e^{i(kx+ly)} + U_R(x, y) \qquad (11)$$

as described in Part I. Here $\tilde{U}_{\text{fit}}$ is the fit amplitude and phase; k and l are the east–west and north–south wavenumbers, and U_R is a residual. In addition, we compute the total inertial kinetic energy from all the measurements, E_{tot}, and the inertial kinetic energy explained by the fit, E_{fit}. Their ratio

$$F_{\text{fit}} = \frac{E_{\text{fit}}}{E_{\text{tot}}} \qquad (12)$$

is the fraction of the inertial energy that can be fit by a plane wave. This ratio will play a key role in our analysis.

All of the fit parameters are shown in Fig. 13 of Part I. The horizontal wavenumber magnitude, for example, increases at a rate βt, reaching about 10^{-5} m^{-1} on day 288.5. In our Fig. 2 we plot F_{fit} for the data (heavy line) along with approximate 95% confidence limits obtained from a Monte Carlo simulation described in the appendix of Part I. Between days 280.5 and 288.5, the period of interest, F_{fit} is always greater than 90%. A single plane wave does an excellent job in describing the spatial structure of the mixed layer currents.

b. *Subinertial currents*

Subinertial currents were estimated along the same drifter trajectories and at three moorings as described in Part I. The two-dimensional field of horizontal velocity and vertical vorticity ζ was computed from all velocity measurements between days 280 and 300 using the Bretherton et al. (1976) objective analysis technique as described in Part I. The point measurements of velocity and the objectively analyzed vorticity fields are shown in Fig. 3.

The objective analysis assumes a steady, nondivergent velocity field. In Part I the absolute vorticity $\zeta_A = \zeta + f$ is shown to lie along the mean streamlines to within the measurement error, consistent with the assumptions of the objective analysis. Along a drifter trajectory, therefore, ζ_A should be constant except for measurement error. This error can be reduced by averaging ζ along a buoy trajectory to form $\langle \zeta_A \rangle$. From this a second, more accurate vorticity estimate $\hat{\zeta}$ can

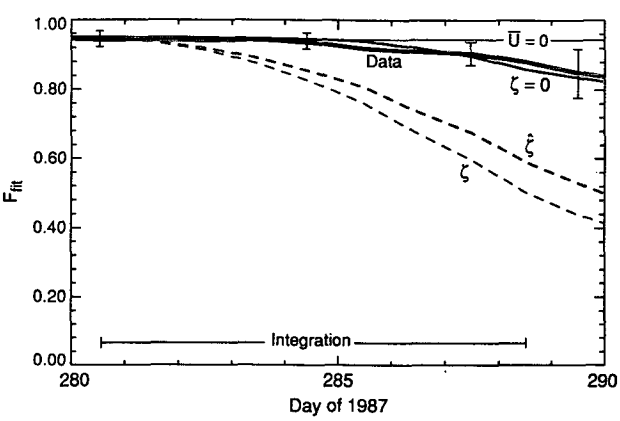

FIG. 2. The fraction of mixed layer energy F_{fit} described by a plane wave for data (heavy line) and four simulations labeled as described in text. Confidence limits are approximately 95% for data.

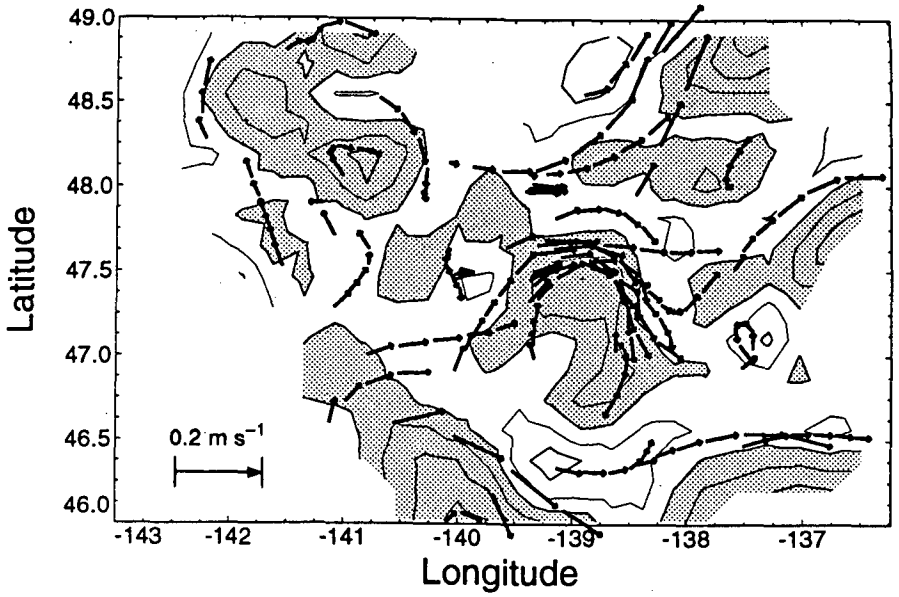

FIG. 3. Subinertial mixed layer velocities (arrows) and objectively analyzed relative vorticity (contours). Vorticity contour interval is 1% of f. Negative vorticity regions are shaded.

be computed, $\hat{\zeta} = \langle \zeta_A \rangle - f$. Our analysis will be made with both ζ and $\hat{\zeta}$.

4. Analysis

The theory was tested by integrating (9) along each drifter trajectory, fitting the results with (11), and comparing the fit parameters with the observations. The initial conditions for the integration were obtained by fitting (11) on day $t_1 = 280.5$ and computing $\tilde{U}(t_1)$ from the fit parameters. The resulting field (Fig. 4a) is very similar to the observed field (Fig. 1a) at the same time. Since these initial conditions imply $F_{\text{fit}} = 100\%$, compared to about 95% in the observations, random noise is added to E_{tot}, reducing F_{fit} by 5%. Four integrations from day 280.5 to day 288.5 were made. The first, assuming no subinertial currents, makes no change in the inertial currents, so the inertial velocity field and fit parameters at day 288.5 are the same as those on day 280.5. This case is labeled "$\bar{U} = 0$" in Fig. 2. The second, assuming $\zeta = 0$, produces the inertial velocity field shown in Fig. 4b and the fit parameters labeled "$\zeta = 0$" in Fig. 2. The third, using ζ, produces the inertial velocity field shown in Fig. 4c and the fit parameters labeled "ζ" in Fig. 2. The fourth, using $\hat{\zeta}$, produces the inertial velocity field shown in Fig. 4d and the fit parameters labeled "$\hat{\zeta}$" in Fig. 2.

The ζ and $\hat{\zeta}$ simulations are inconsistent with the data. In both cases, the simulated backrotated inertial vectors on day 288.5 contain more small-scale variability than is observed. This variability is due to the modulation of f_{eff} by the vorticity. Numerically, rms relative vorticity of $0.02f$ should produce rms variations in the direction of the backrotated inertial vectors on day 288.5 of 40° rms. This is clearly seen in Figs. 4c and 4d. These modulations occur on the scale of the vorticity, which is much smaller than the scale of the inertial motions. They therefore degrade the fit of (11). By day 288.5, F_{fit} is reduced to about 60%, a value about five times less than is observed (Fig. 2).

The $\zeta = 0$ case produces the best fit with the data, fitting the observed decrease in F_{fit} nearly perfectly. Some of the decrease in F_{fit} could be due to the decrease in E_{tot}, which is not modeled by (9), so this fit may be artificially good. Although not shown, this simulation does not change k and varies l as $-\beta t$ and thus also fits observed wavenumbers well.

Internal wave propagation effects have not been included in (9). Equation (10) indicates that if additional small-scale variability in the inertial currents was generated by the subinertial vorticity, corresponding small-scale variations in the wave propagation rate should occur. For example, the strong gradient in the center of the array in Figs. 4c and 4d corresponds to a local wavelength $2\pi\tilde{k}^{-1}$ of about 200 km. This $\tilde{k}$ is about three times the observed $\tilde{k}$, so (10) predicts that the rate of wave propagation would locally be about nine times larger, removing half the mixed layer inertial current energy in about a day. Thus, if wave propagation had been included in (9), the small-scale variability in the mixed layer currents in the ζ and $\hat{\zeta}$ cases would have been even larger and would have disagreed even more strongly with the observations.

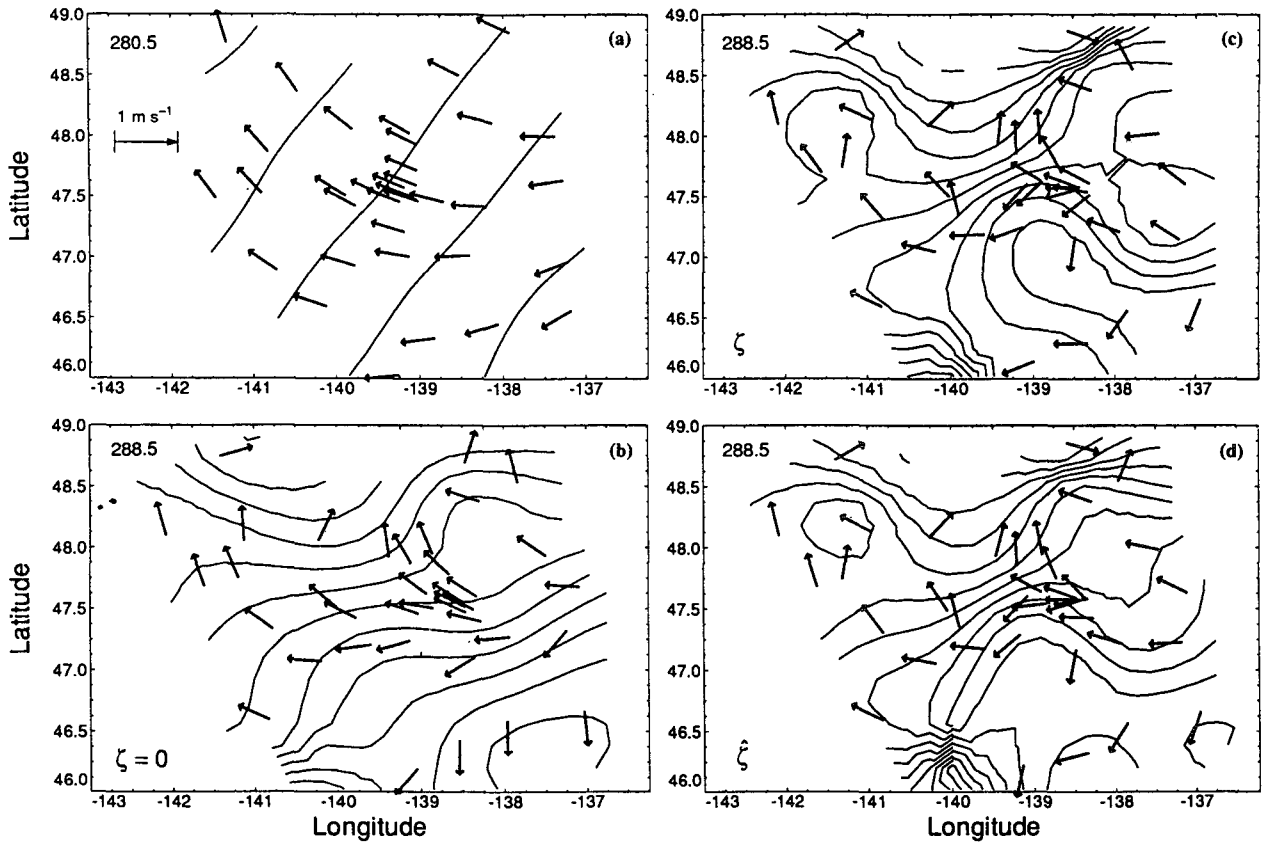

FIG. 4. Simulated mixed layer backrotated inertial current vectors: (a) initial conditions, day 280.5, and (b–d) predicted vectors on day 288.5 for three simulations as labeled. Vector direction is contoured with interval of 22.5°.

5. Supporting evidence

An analysis in Part I yields similar results. By day 297, the mixed layer inertial currents have mostly propagated out of the mixed layer and into the thermocline. These thermocline inertial currents have nearly the same dominant horizontal wavenumber as the mixed layer inertial currents from which they form. The variability in their spatial structure is significantly larger than that of the mixed layer currents, comparable to that seen in Figs. 4c and 4d (see Part I, Fig. 18). However, it is still much less than would be expected from the variations in ζ acting over 21 days.

In Part II, a two-dimensional numerical model is used to directly simulate the evolution of mixed layer inertial currents in the presence of subinertial currents of magnitude and vorticity comparable to those observed. This simulation includes wave propagation and nonlinearity, but it cannot properly simulate horizontal advection. In contrast, the simulation made here, (9), includes horizontal advection, but not wave propagation or nonlinearity. Both simulations include f_{eff}, and both predict small-scale variations in inertial currents that are much larger than observed, reducing F_{fit} to about 60% in 10 days. In both, setting $\zeta = 0$ yields a better agreement between the model and the observations.

6. Summary

The near-surface velocity field in a 300 km × 300 km region of the northeast Pacific was measured using an array of 36 nearly Lagrangian drifters drogued at 15 m, and 3 ADCP moorings as described in Part I. A storm generates strong inertial currents in the mixed layer. In this paper, the effect of the subinertial currents on the evolution of the horizontal structure of these near-inertial frequency currents is analyzed. Linearized theory predicts that the frequency of these currents will be shifted by $\frac{1}{2}\zeta$, where ζ is the relative vorticity of the subinertial flow, and that they will be advected by the subinertial flow. The advection should make only small, marginally detectable changes in the structure of the inertial currents. Changes similar to those predicted are observed. The frequency variation, about 1%, should lead to a strong modulation of the phase of the mixed layer inertial currents. Such modulations are not observed. The best agreements with the observations,

both here and in Part II, are obtained by ignoring the subinertial vorticity.

7. Discussion

The failure of the inertial currents to respond to the subinertial vorticity is surprising. The effect of vorticity on inertial currents has been clearly documented in other studies, so it seems unlikely that it would not be operating here. However, the rms vorticity here is much smaller than in Kunze and Sanford (1984) or Mied et al. (1987), so other competing effects may be proportionally stronger here.

The vorticity field was computed from velocity data using objective analysis and assuming that vorticity is smoothly distributed. With this type of analysis, it is difficult to see how the rms vorticity could be reduced to 20% of the value used here. Furthermore, both the ζ and $\hat{\zeta}$ fields yield similar results. Alternatively, the vorticity could be concentrated in fronts that are much smaller than the typical spacing of our velocity data. In this case, $\zeta = 0$ would be a good assumption for most locations and almost all of the inertial currents would behave as if there were no subinertial vorticity. This is consistent with our observations.

Nonlinear wave–wave interactions either between inertial motions or with higher-frequency internal waves could possibly act to horizontally homogenize the near-inertial motions. A better understanding of these interactions is needed before this hypothesis can be tested.

These results, like those from Parts I and II, caution us that, although the physics of near-inertial motions appears to be well understood theoretically in terms of linear theory and linear interactions with subinertial motions, our knowledge may not yet be complete enough for accurate predictions of their evolution to be possible. Even if operational models could produce accurate mesoscale vorticity fields and could accurately predict the generation of near-inertial motions by the wind, the uncertainties in the physics of near-inertial motions may still limit the accuracies of the predictions produced by present models.

Acknowledgments. This work was supported by the Office of Naval Research under Contracts N00014-84-C-0111 and N00014-87-K-0004, and Grant N00014-90-J-1104.

REFERENCES

Bretherton, F. P., R. E. Davis, and C. B. Fandry, 1976: A technique for objective analysis and design of oceanographic experiments applied to MODE-73. *Deep-Sea Res.*, **23,** 559–582.

Crawford, G. B., and W. G. Large, 1995: A numerical investigation of resonant inertial response of the ocean to wind forcing. *J. Phys. Oceanogr.*, submitted.

D'Asaro, E. A., 1995: Upper ocean inertial currents forced by a strong storm. Part II: Modeling. *J. Phys. Oceanogr.*, **25,** 2937–2957.

——, C. C. Eriksen, M. D. Levine, P. Niiler, C. A. Paulson, and P. Van Meurs, 1995: Upper ocean inertial currents forced by a strong storm. Part I: Data and comparisons with linear theory. *J. Phys. Oceanogr.*, **25,** 2909–2936.

Kunze, E., 1985: Near-inertial wave propagation in geostrophic shear. *J. Phys. Oceanogr.*, **15,** 544–565.

——, E., and T. B. Sanford, 1984: Observations of near-inertial waves in a front. *J. Phys. Oceanogr.*, **14,** 566–581.

——, E., R. Schmitt, and J. M. Toole, 1994: The energy balance in a warm-core ring's near-inertial critical layer, *J. Phys. Oceanogr.*, **25,** 942–957.

Large, W. G., and G. B. Crawford, 1995: Observations and simulations of upper-ocean response to wind events during the Ocean Storms experiment. *J. Phys. Oceanogr.*, **25,** 2831–2852.

Levine, M. D., and V. Zervakis, 1995: Near-inertial wave propagation into the pycnocline during Ocean Storms: Observations and model comparison. *J. Phys. Oceanogr.*, **25,** 2890–2908.

Mied, R. P., G. J. Lindemann, and C. L. Trump, 1987: Inertial wave dynamics in the North Atlantic Subtropical Zone. *J. Geophys. Res.*, **92,** 13 063–13 074.

Qi, H., R. A. de Szoeke, C. A. Paulson, and C. C. Eriksen, 1995: The structure of near-inertial waves during Ocean Storms. *J. Phys. Oceanogr.*, **25,** 2853–2871.

Zervakis, V., and M. D. Levine, 1995: Near-inertial energy propagation from the mixed layer: Theoretical considerations. *J. Phys. Oceanogr.*, **25,** 2872–2889.